Medical Engineering and Physics 125 (2024) 104120

Contents lists available at ScienceDirect

Medical Engineering and Physics

journal homepage: www.elsevier.com/locate/medengphy

Paper

Novel tetrapolar single-needle electrode for electrochemotherapy in bone cavities: Modeling, design and validation

Lucas B. Lopes [a,*], Guilherme B. Pintarelli [a,b], Raul Guedert [a], Daniella L.L.S. Andrade [a], Afrânio C. Antonio [a], Clara T.S. Ramos [a], Jéssica R. da Silva [a], Marcelo M.M. Rangel [c], Daniela O.H. Suzuki [a]

[a] Institute of Biomedical Engineering, Federal University of Santa Catarina, Florianópolis, 88040-900, SC, Brazil
[b] Department of Control and Automation Engineering, Federal University of Santa Catarina, Blumenau, 89036-004, SC, Brazil
[c] Oncology Veterinary, VetCâncer, São Paulo, 04523-013, SP, Brazil

ARTICLE INFO

Keywords:
Electroporation
Electric field
Bone cavity
Single needle
Cancer

ABSTRACT

Electrochemotherapy is a cancer treatment in which local pulsed electric fields are delivered through electrodes. The effectiveness of the treatment depends on exposing the tumor to a threshold electric field. Electrode geometry plays an important role in the resulting electric field distribution, especially in hard-to-reach areas and deep-seated tumors. We designed and developed a novel tetrapolar single-needle electrode for proper treatment in bone cavities. *In silico* and *in vitro* experiments were performed to evaluate the electric field and electric current produced by the electrode. In addition, tomography images of a real case of nasal cavity tumor were segmented into a 3D simulation to evaluate the electrode performance in a bone cavity. The proposed electrode was validated and its operating range was set up to 650 V. In the nasal cavity tumor, we found that the electrode can produce a circular electric field of 3 mm with an electric current of 14.1 A at 500 V, which is compatible with electrochemotherapy standards and commercial equipment.

1. Introduction

Electrochemotherapy (ECT) is a cancer treatment that combines chemotherapeutic agents and electroporation (EP) to enhance drug cytotoxicity [1–3]. EP is a phenomenon that occurs when cells are exposed to an appropriate pulsed electric field (PEF), which increases cell permeability. This technique is currently explained by the appearance of aqueous pores within the cell membrane [4,5]. Depending on the PEF intensity (*i.e.*, the combination of amplitude, pulse duration, number of pulses, and repetition rate), EP can occur in a reversible manner, where pores close after PEF application and cell homeostasis are restored, or irreversibly, where the high intensity of PEF leads to cell death [6,7]. In ECT, locally increased permeabilization by reversible electroporation (RE) facilitates drug delivery to tumor cells [8]. Due to the complex electric field distribution in ECT, it is expected to some extent of irreversible electroporation (IRE) at surrounding regions. The IRE may provoke tissue reduction by apoptosis and/or necrosis which is undesired when operating ECT [9].

The PEF is delivered by EP devices via electrodes that are directly related to the resulting electric field distribution. The European Standard Operating Procedures on Electrochemotherapy (ESOPE) [10,11] standardize treatment procedures for primary skin cancer and skin metastases of any histology and recommends four types of electrodes. ESOPE electrodes are divided into plate electrodes, recommended for the treatment of small superficial tumors, and needle electrodes, which can reach deeper areas and are recommended for small and larger tumors. Other treatment regions are being studied and there is an increasing demand for treatments in hard-to-reach regions and deep-seated tumors [12,6] for which ESOPE electrodes may not be the best choice or even suitable to generate the necessary electric field distribution [13,14].

The electric field is a critical parameter in ECT treatment as tumor regions with insufficient PEF (*i.e.*, under reversible electroporation threshold) may lead to tumor recurrence and treatment failure [15–17]. Bone cavities (*i.e.,* bone structures with air-filled cavities, such as nasal cavity and paranasal sinuses) present a challenge for ECT due to the insulating behavior (*i.e.*, very low conductivity) of bones and the presence of air, which can lead to electric field diffraction [18–20]. In addition,

* Corresponding author.
E-mail address: lucas.bertinetti@posgrad.ufsc.br (L.B. Lopes).

https://doi.org/10.1016/j.medengphy.2024.104120
Received 17 August 2023; Received in revised form 12 January 2024; Accepted 14 February 2024
Available online 21 February 2024
1350-4533/© 2024 IPEM. Published by Elsevier Ltd. All rights reserved.

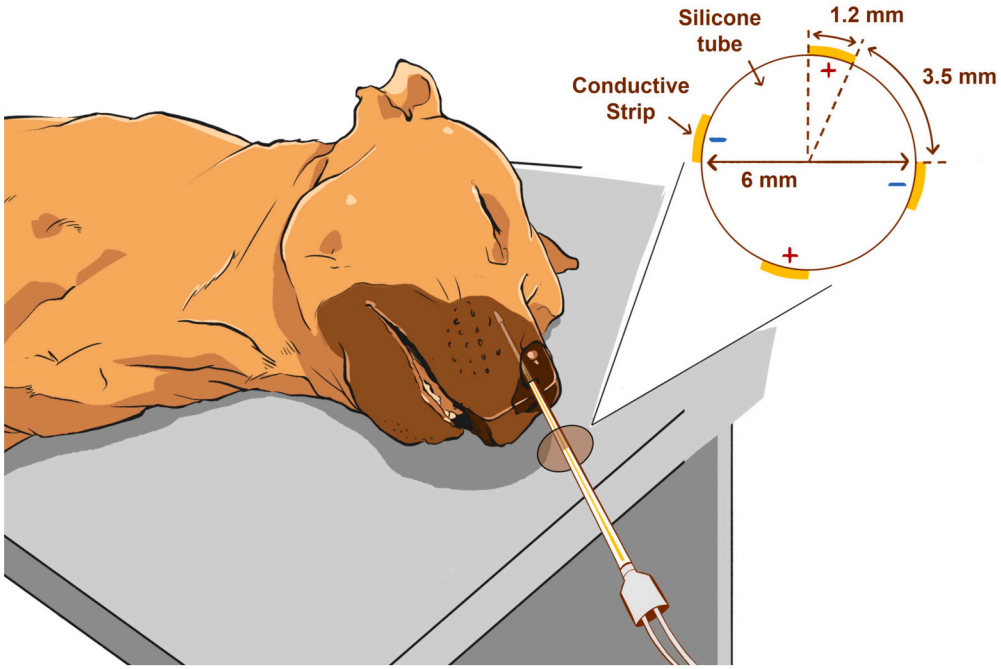

Fig. 1. Proposed electrode dimensional schematic. The conductive strips fill 25% of the silicon tube circumference. The polarity of each strip is indicated by a red plus sign (positive polarity) and a blue minus sign (negative polarity).

standard ESOPE electrodes are generally unable to treat tumors in bone cavities [18]. In recent years, different electrode designs were proposed [21,22].

Vegetable models such as potato tubers (*Solanum tuberosum*) have been used as an alternative EP phantom as part of the 3Rs (Replacement, Reduction, and Refinement) practice because they provide rapid visual feedback on the efficacy of EP [23]. EP stimulates the production of brown pigment through oxidation of potato tissue (*i.e.*, the interaction between polyphenol oxidase enzymes and phenolic substrates), resulting in a dark stained area where EP occurs. Therefore, it is possible to assess not only the effectiveness of EP, but also how the electric field was distributed in the tissue [24]. In addition, numerical models and simulations are a tool for the analysis of the electric field and current in ECT, that take into account the nonlinear increase in tissue conductivity due to EP [25–27].

In this work, we modeled and developed a tetrapolar single-needle electrode for ECT in bone cavities. The desired result was to create a circular PEF around the electrode that would allow minimally invasive treatment of bone cavities. Different design approaches were evaluated prior to manufacturing the device. Subsequently, *in silico* and vegetable *in vitro* experiments were performed to evaluate the resulting electric field distribution and electric current under different voltages. These tests allowed the validation and definition of the operating range of the electrode. Finally, computed tomography (CT) images of a canine tumor in the nasal cavity were segmented into a 3D simulation study of the electric field coverage and electrode limitations.

2. Methods

The tetrapolar single-needle electrode consists of four conductive strips of gold-plated copper arranged in an insulating solid silicone tube (Fig. 1) (Patent number: BR 102021019917-2 A2). Before the fabrication of the electrode, numerical simulations were performed to evaluate the percentage coverage of the tube circumference by the conductive strips. In this model, the *in silico* electric current was calculated in the tumor tissue. After electrode fabrication, an *in vitro* study was performed in *Solanum tuberosum* tissue to evaluate the performance and validate the proposed electrode. Then, CT-based simulations of a tumor in the nasal cavity were performed to analyze the electrode performance in a bone cavity environment.

2.1. Numerical models and simulations

The software COMSOL Multiphysics version 5.1 (COMSOL Inc., Stockholm, Sweden) was used to perform the numerical studies using the electric currents module and the stationary mode. The tissues were considered homogeneous and isotropic and the Laplace equation (1) was solved. Vectors are expressed in bold.

$$-\nabla \cdot (\sigma \cdot \nabla \Phi) = 0 \tag{1}$$

where $\nabla \cdot \ [1/m]$ is the divergence, $\sigma \ [S/m]$ is the electrical conductivity of the medium, $\nabla \ [1/m]$ is the gradient, $\Phi \ [V]$ is the scalar electric potential.

The electric field is solved by the negative gradient of potential (2) and the electric current density is solved by Ohm's law (3).

$$\boldsymbol{E} = -\nabla \Phi \tag{2}$$

$$\boldsymbol{J} = \sigma \boldsymbol{E} \tag{3}$$

where $\boldsymbol{E} \ [V/m]$ is the electric field and $\boldsymbol{J} \ [A/m^2]$ is the electric-current density.

The steady-state regime was considered and Dirichlet and Neumann boundary conditions were applied. Dirichlet is applied to define a fixed scalar potential in boundaries between the electrode and the medium. Neumann is applied to define zero electric current density at the outer surface of the model geometry [28,20,29].

The tissue conductivity was modeled by the sequential model from Sel et al. [30]. This model consists of a sequence of static models that relates the tissue conductivity to electric field intensity by a sigmoid function (Eq. (4)) in steady-state regime. The sequential model performs a simplification from the time domain to the static domain that reduces computational complexity and is widely used in ECT simulation [8,31,13].

$$\sigma(E) = \sigma_0 + \frac{\sigma_{max} - \sigma_0}{1 + D \cdot e^{-\left(\frac{E-A}{B}\right)}} \tag{4}$$

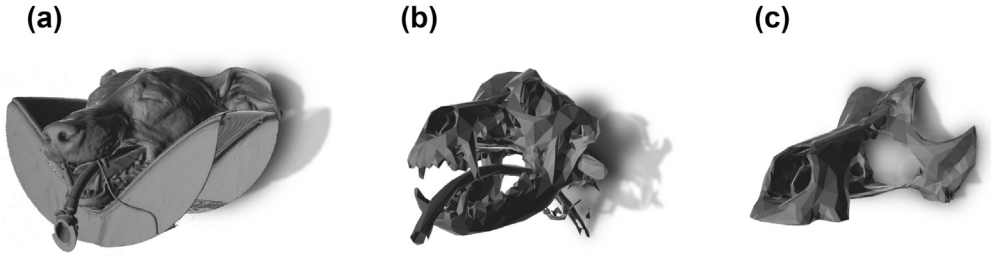

Fig. 2. CT image segmentation steps. **(a)** considering all tissues, **(b)** only the bone tissue (note that the tube is retained once it is the same color as the bone tissue), and **(c)** only the region of interest.

Table 1
Electrical parameters of tissues and materials used in *Solanum tuberosum* and tumor simulations.

Material	Electrical Conductivity [S/m]		Electric Field [kV/m]	
	σ_0	σ_{max}	E_{re}	E_{ire}
Potato Tissue	0.03	0.36	20	80
Tumor	0.30	0.75	20	80
Bone	0.01	-	-	-
Air	$1{\cdot}10^{-20}$	-	-	-
Stainless steel	$1.74{\cdot}10^{6}$	-	-	-

where,

$$A = \frac{E_{ire} + E_{re}}{2},\ B = \frac{E_{ire} - E_{re}}{C},\ C = 8 \text{ and } D = 10$$

The parameter σ_0 represents the initial conductivity before the pulse application (*i.e.,* the natural conductivity), σ_{max} is the maximum conductivity reached at the end of the pulse application, E_{re} is the reversible electric field threshold, and E_{ire} is the irreversible electric field threshold. The electric field thresholds set the transition zone between initial and final conductivity. These parameters are found for each type of biological tissue from in vivo or ex vivo experiments. From measurements of current and voltage applied to biological tissue, its conductivity is calculated and modeled as a function of the electric field. The potato model was proposed by Suarez et al. [32] and compared to three other models, presenting the best results [33]. Tumor model was proposed by Corovic et al. from B16 and LPB sarcomas and the electric field thresholds were assessed by ^{51}CrEDTA indicator [28]. The conductivity of the bone tissue was assumed to be constant. This is a typical approach when simulating bone tissue as there is little EP experimental data available [34–36]. The parameters of the potato tissue, tumor, bone, air, and stainless steel (data from the COMSOL library) are listed in Table 1.

Simulations of the electrode circumference coverage were performed in tumor tissue. The different ranges of the electrode circumference are shown in Supplementary Fig. S1. The 3D geometry is shown in Supplementary Fig. S2. The electrode validation simulations were performed in *Solanum tuberosum* tissue and the 3D geometry is the same as the electrode circumference coverage simulations (see Supplementary Fig. S2). The finite element mesh was automatically created by the COMSOL mesh generation tool in the 'finer' resolution. This procedure results in an optimized mesh with small mesh elements around the electrode, increasing the accuracy in this area (see Supplementary Fig. S3). The complete mesh consisted of 187351 domain elements, 14122 boundary elements, and 1563 edge elements.

2.2. Case study and CT image segmentation

A 12-year-old male dog was diagnosed with carcinoma in the nasal cavity. The CT images were used to create the geometry model of the nasal cavity. The CT images were segmented using a custom segmentation script based on ITX library (https://doi.org/10.5281/zenodo.3592082) [37,38] (Fig. 2). The 3D images were then imported to Blender 3.1 software (Blender Foundation, the Netherlands; https://www.blender.org), where 1 mm of bone margin was homogeneously added to the whole bone tissue. The bone layer was added because there were thin regions that were not covered by the finite element mesh (a finer mesh). The geometry model (STL format) was then subjected to a mesh simplification algorithm (Mesh Decimate) and exported via Mesh Node into COMSOL Multiphysics v.5.1, in which it was then converted to a solid geometry as a 3D geometry component (see Supplementary Fig. S4). The complete mesh consisted of 79698 domain elements, 11154 boundary elements, and 1547 edge elements. After verifying that the tumor would be covered by the electric field, the tumor size was increased. This approach was used to evaluate the maximum electric field coverage delivered by the electrode in the tumor tissue.

2.3. In vitro study

EP stimulates the oxidation of vegetable tissue and the production of brown pigment. After the EP application, the dark stained area indicates EP success and changes in electric field distribution [20]. Because of this, vegetable tissues has been used as EP phantom [24].

The vegetable tissue used in the *in vitro* experiments was the potato tuber (*Solanum tuberosum*). The potatoes were purchased from a local grocery store on the day of the experiments. The potato samples were not peeled and were incised where the electrode was to be inserted (*i.e.,* to mimic the cavity). The potatoes were approximately 8x larger then the electrode, which ensured that the samples are large enough so that the edges did not affect the electric field distribution. The ESOPE protocol (eight squared pulses of 100 µs with a repetition rate of 1 Hz) [39] at voltages of 500 V, 650 V, and 800 V was applied to all potato samples using a custom electroporation device [33]. The electrode was inserted 40 mm into the potato samples. The sample size was 7 elements (N = 7) for each voltage. A control group (N = 7) was tested using the same procedure as the EP groups but without applying any voltage. The surfaces of the samples were dried before and after pulse application and the samples were stored in a sealed container on a paper towel moistened with 3 ml of 4% citric acid for 24 hours at a room temperature of 25 °C. These procedures minimize the tissue oxidation caused by the natural liquid released by the potato and in the region that is in contact with the air. As a result, the non-EP effects do not compromise the tissue staining [20,29]. After 24 hours, the samples were cut open perpendicular to the electrode plane and photographed with a cell phone camera (SonyEricsson K790C, 3.2-megapixel camera, digital zoom: 16x; autofocus) in a controlled light chamber. Potato dark-stained areas were measured using ImageJ software (National Institute of Health, USA, https://imagej.net/) without image processing. Voltage and current measurements during the application of the EP protocol for each sample were recorded using the Tektronix A621 Current Probe and Tektronix DPO2012B Oscilloscope (Tektronix, Inc., USA).

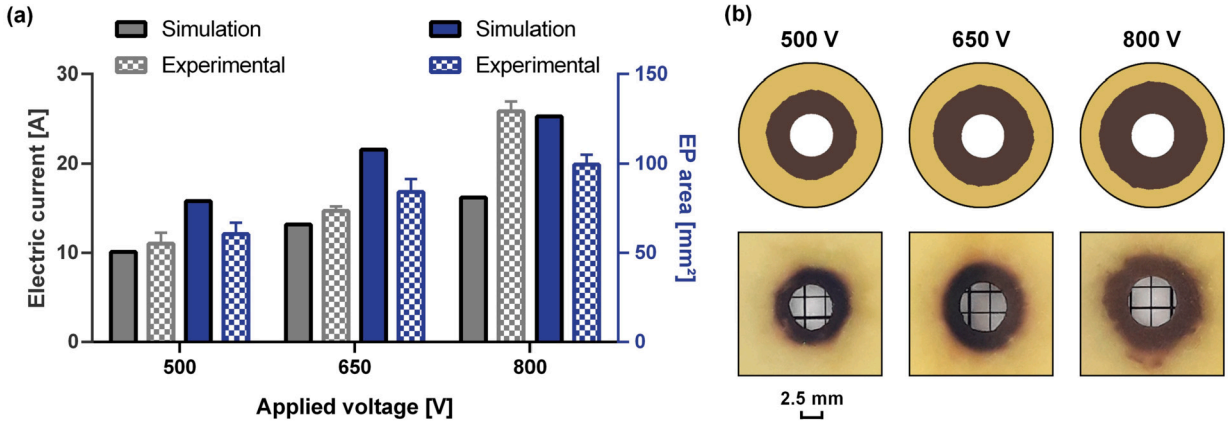

Fig. 3. Numerical and *in vitro* results of electrode evaluation for 500 V, 650 V, and 800 V. **(a)** *In silico* and *in vitro* electric currents during EP application and EP affected areas. *In vitro* measurements are shown as mean values and CI = 0.95 (vertical bars). **(b)** *In silico* electric field distribution and *in vitro* dark stained region in *Solanum tuberosum*. The brown area represents is the area in which EP occurs. The proportions between *Solanum tuberosum* samples and the *in silico* results were preserved.

2.4. Data analysis and statistics

The dataset for the *in vitro* experiments has EP areas and electric currents for 500 V, 650 V, and 850 V, resulting in 6 data groups. Each data group from the EP area and current was compared in order to determine whether there was a significant difference between groups. The purpose of this was to ensure that the sample size was enough. *In silico* EP areas and electrical currents were also compared to the corresponding *in vitro* mean of each data group. Each data group was subjected to the Shapiro-Wilk normality test with a confidence level of 95% (CI = 0.95). To test means, the data must be normally distributed. All groups were found to be represented by a normal distribution (see Supplementary Table S6). No data transformation was performed to fit the normal distribution. The data were then subjected to an unpaired t-test with Welch's correction (without assuming equal standard deviations) with a confidence level of 95% (CI = 0.95), which indicated a significant difference between the groups (see Supplementary Table S7). The t-test was chosen because of the small sample size (n = 7 samples). The relative error (*i.e.,* the percentage difference between the mean EP area and current of each experimental group and the *in silico* value) was calculated in order to compare the *in vitro* and simulated data (see Supplementary Table S4 and S5). The statistical software package RStudio (RStudio v. 1.2, Inc, 2019, https://www.rstudio.com/products/rstudio/) was used to perform all data analyses.

2.5. Ethics declarations

Following the Animal Welfare Act and the Public Health Policy on the Humane Care and Use of Laboratory Animals, ethical review and approval by the Institutional Animal Care and Use Committee (IACUC) are not required for nonintrusive projects that do not involve manipulation of the animal or its environment, or the study is only observational (https://animalcare.umich.edu/institutional-animal-care-use-committee). The Conselho Nacional de Controle de Experimentação Animal (CONCEA) in Brazil indicates that a case report treated in an animal hospital is not classified as an animal experiment and therefore does not require ethical review and approval (https://www.gov.br/mcti/pt-br/composicao/conselhos/concea). Therefore, no ethical review by the Statement Animal Experiment Committee was required for the use of veterinary examination images. In addition, the authors state that there was no interference with decisions regarding the treatment of the animal and that the examination images were used after the treatment was completed. This study also complies with relevant institutional, national, and international guidelines and laws on experimental research and field studies on plants or plant material.

3. Results

3.1. Assessment of electrode circumference coverage before fabrication

The dimensions of the conductive strip were defined as 40 mm in height (along the silicone tube), and the width was chosen based on simulations of the electric current in tumor tissue. The coverages of 25%, 50%, or 75% of the electrode circumference (*i.e.,* the needle surface) were tested. The choice of electrode configuration took into account the EP volume and the electric current. The 25% electrode perimeter coverage was selected for presenting lower values of current. The electrode design data can be found in Supplementary Table S1 and Supplementary Figs. S1 and S2. The electrode dimensions are shown in Fig. 1.

3.2. In vitro experiments for electrode design validation

Fig. 3a shows a comparison of electric current and EP area from *in silico* and *in vitro* studies (mean and CI = 0.95). Fig. 3b shows a comparison between the distribution of electric fields from the *in silico* study and the dark stained areas of *Solanum tuberosum* found in the *in vitro* study. Dark areas of the potato indicate where EP occurred. Data from Fig. 3 can be found in Supplementary Tables S2, S3, S4, and S5. The control samples did not present any dark stained areas.

3.3. Nasal cavity tumor simulation

Fig. 4a-b shows the electric field distribution in the CT-based geometry. This case study shows the presence of a bone protuberance (indicated by dashed circles). Fig. 4c shows another scenario in which a bone gap with a diameter of 3 mm, 6 mm, and 7 mm was simulated. The regions with insufficient electric fields were indicated by arrows.

4. Discussion

Traditional ECT electrodes (*e.g.,* two parallel plates and an array of needles) were developed for the treatment of cutaneous and subcutaneous tumors [40,11,41]. However, there is an increasing demand for ECT of hard-to-reach areas and deep-seated tumors, leading to the research of new electrode designs [13,12,42,22,43]. This type of development is seen in other electroporation-based therapies [44,45]. The development of the tetrapolar single-needle electrode was motivated by the need for a suitable electrode to treat a canine tumor in the nasal cavity. Effective new electrodes must provide a suitable electric field distribution and preferably a less invasive treatment route. In this case, the single-needle electrode is less invasive because fewer incisions may

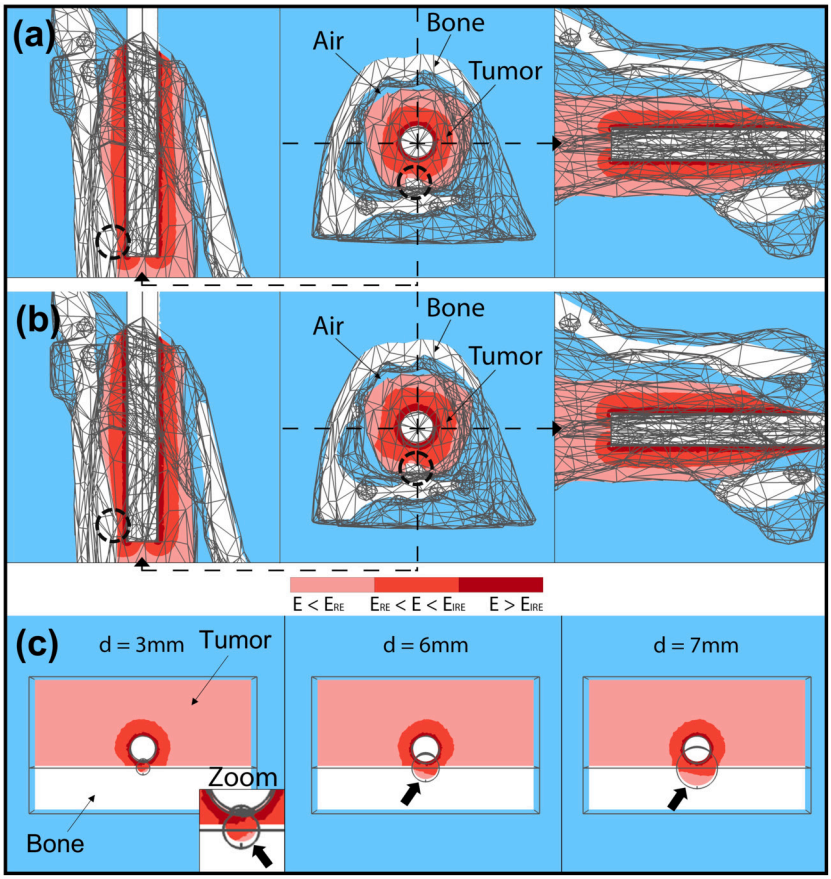

Fig. 4. Distribution of the electric field for the studied geometries. Light red areas represent electric field under RE threshold, red areas represent RE electric fields and dark red areas represent IRE electric fields. The top and middle panels show the result for 500 V **(a)** and 650 V **(b)** for the CT-extracted geometry. Dashed circles indicate the presence of bone protuberance in the nasal cavity. In the lower panel, the geometry represents a bone gap with diameters of 3, 6, and 7 mm for 500 V **(c)**. The regions with insufficient electric field are indicated by arrows. The sectional planes were generated using COMSOL Multiphysics v.5.1.

be required. In addition, the tetrapolar configuration was chosen after assessing that a bipolar configuration might not be able to generate an adequate electric field in nasal cavities [46].

Ensuring sufficient coverage of the target tissue with a local electric field is one of the most significant problems in the development of new electrodes [47,48,43,29]. In this work, the goal was to develop an electrode capable of generating an uniform circular electric field around its single needle. During the electrode design step, we performed simulations to decide how much of the electrode circumference would be covered by the conductive strips. We chose the 25% coverage over 50% or 75% coverage due to the minimal difference in the EP volume (11% and 15%, respectively) and considerable difference in electrical current (56% and 139%, respectively) in which the currents remained close to the standard specification of ECT pulse devices. The high currents (>50 A) are incompatible with commercially available ECT equipment and may damage the biological tissue [49,50].

Solanum tuberosum is a valuable tool for testing new types of electrodes [51,23] as the vegetable tissue complies with the 3Rs concept of animal welfare in research [33] and it is recommended to avoid the use of animals in ECT experimental tests. This work was directed toward the design, manufacture, and validation of a new electrode, as well as the study of its operating range. It is of utmost importance that these *in silico* and *in vitro* tests are performed before any *in vivo* experimentation, as the probability of treatment failure is high and animals may suffer.

The electrode evaluation showed agreement between the potato samples and the simulation (Fig. 3b), indicating that it was possible to generate a circular electric field around the needle. The average EP area seen in the potato samples was 21.4% to 23.4% smaller than in the simulations (Fig. 3a and Supplementary Table S4). This type of variation is to be expected because the browning effect tends to be smaller as the electric field approaches the RE threshold because less intracellular fluid leaks out and consequently less tissue is oxidized. Furthermore, a homogeneous tissue is simulated, but the potato's inner medulla (*i.e.,* the inner part, where the electrode is inserted) is known to have more free amino acids, resulting in slightly higher conductivity [24,52,33]. There are difficulties in accurately predicting the electric field coverage in ECT treatments, but a voltage margin is usually applied to compensate for uncertainties in the simulations [28]. Electric current errors were less than 12% for 500 V and 650 V. However, for 800 V, the current error was 53.7% (Fig. 3a and Supplementary Table S5), indicating that the model cannot predict the current for higher voltages (>650 V) for the proposed electrode. Monitoring the electrical current with each pulse allows the evaluation of EP. The current is expected to rise with each pulse due to the increase in tissue conductivity caused by EP. The average current increased from the first to the eighth pulse due to the EP effect [53,54] at 500 V and 650 V. At 800 V, this effect was not seen because the current saturated at the first pulse (see Supplementary Fig. S5). At this voltage, it is suspected that irreversible electroporation occurred in a larger tissue region than predicted by the simulation.

The application of ECT in paranasal cavities with ESOPE electrodes represents a challenge due to the limited access, in which plate and needle electrodes may require surgery to expose the tumor and multiple applications to cover the tumor, and the complex anatomy involving soft and bone tissues which can lead to inhomogeneous electrical fields whenever the electrode edges are close to the bone [55–57,18,19]. We assessed how the proposed electrode generates an electric field in a realistic simulation of a bone cavity. After determining that the electrode

delivered a sufficiently high electric field to the original tumor, the tumor was arbitrarily enlarged to achieve maximum electrode coverage. This procedure was used because the tumor was surrounded by air, so the electric field could not propagate beyond the tumor. By increasing the tumor size sufficiently so that the tumor edges did not have a sufficient electric field to cause EP, it was possible to evaluate how much of this region would be covered by the proposed electrode. The simulations showed an electric field coverage of 3 mm at 500 V and 4 mm at 650 V around the electrode (Fig. 4a-b). The treatment was considered effective if the target area was above the RE threshold around the electrode. The tumor region is surrounded by air. The air volume between the tumor and the bone cavity was reduced after the addition of the bone margin. However, this procedure did not affected the electric field distribution in the tumor since it is still surrounded by air. We believe that the bone margin would affect the results if it was large enough to cover the entire air region. We discarded the voltage of 800 V due to the current model deviation. The current increased by 35% between the 500 V and 650 V voltages (simulated current of 14.1 and 19.1 A, respectively). The electric current values were compatible with the specifications of commercial ECT pulse delivery devices [49,50]. The single-needle electrode presents an advantage over ESOPE electrodes as it is adapted to the anatomy of the paranasal cavity, requiring fewer incisions and applications, and providing a more robust electric field distribution in relation to interference caused by bone tissue, since the circular electric field is applied from inside to outside of the tumor.

Images from CT showed the presence of a bone protuberance in the nasal cavity of the canine patient. Protuberances are known to cause electric field diffraction [20]. Nevertheless, the protuberance did not affect the treatment in this case. From the same perspective of field diffraction around bones, we were encouraged to simulate a bone gap (Fig. 4c), which is an anatomical element found in cavities and bone structures. The results showed an insufficient electric field at the bottom of the bone gap for the three different sizes of the gap. Incomplete or ineffective electric field coverage may lead to ECT failure and tumor recurrence [14]. Realistic simulations based on imaging studies allow for target treatment planning and the detection of potential problems. These results are the first step toward *in vivo* testing.

5. Conclusion

The tetrapolar single-needle was designed, fabricated and validated for voltages between 500 V and 650 V. This article discusses an electrode that is effective in treating the nasal cavity. It requires a minimum voltage of 500 V. At this voltage, the effective treatment distance around the electrode is 3 mm and the electric current is within the standards for ECT treatment.

CRediT authorship contribution statement

Lucas B. Lopes: Conceptualization, Data curation, Formal analysis, Investigation, Methodology, Validation, Visualization, Writing – original draft, Writing – review & editing. **Guilherme B. Pintarelli:** Conceptualization, Formal analysis, Investigation, Writing – review & editing. **Raul Guedert:** Software, Validation, Visualization, Writing – review & editing. **Daniella L.L.S. Andrade:** Data curation, Investigation, Methodology, Visualization, Writing – review & editing. **Afrânio C. Antonio:** Investigation, Resources, Validation, Visualization, Writing – review & editing. **Clara T.S. Ramos:** Data curation, Visualization, Writing – review & editing. **Jéssica R. da Silva:** Data curation, Visualization, Writing – review & editing. **Marcelo M.M. Rangel:** Conceptualization, Funding acquisition, Resources, Visualization, Writing – review & editing. **Daniela O.H. Suzuki:** Conceptualization, Funding acquisition, Supervision, Visualization, Writing – review & editing.

Data availability

All data generated or analyzed during this study are included in this article (and its Supplementary Information files).

Acknowledgements

Funding: This work was supported by Coordenação de Aperfeiçoamento de Pessoal de Nível Superior (CAPES) and Conselho Nacional de Desenvolvimento Científico e Tecnológico (CNPq) which provided doctoral and master's scholarships. The funding sources had no involvement in this work.

Appendix A. Supplementary material

Supplementary material related to this article can be found online at https://doi.org/10.1016/j.medengphy.2024.104120.

References

[1] Šemrov D, Miklavčič D. Calculation of the electrical parameters in electrochemotherapy of solid tumours in mice. Comput Biol Med 1998;28(4):439–48. https://doi.org/10.1016/S0010-4825(98)00017-1.
[2] De Virgilio A, Ralli M, Longo L, Mancini P, Attanasio G, Atturo F, et al. Electrochemotherapy in head and neck cancer: a review of an emerging cancer treatment. Oncol Lett 2018;16(3):3415–23. https://doi.org/10.3892/ol.2018.9140.
[3] Esmaeili N, Friebe M. Electrochemotherapy: a review of current status, alternative igp approaches, and future perspectives. J Healthc Eng 2019:2019. https://doi.org/10.1155/2019/2784516.
[4] Weaver JC, Chizmadzhev YA. Theory of electroporation: a review. Bioelectrochem Bioenerg 1996;41(2):135–60. https://doi.org/10.1016/S0302-4598(96)05062-3.
[5] Kotnik T, Kramar P, Pucihar G, Miklavcic D, Tarek M. Cell membrane electroporation-part 1: the phenomenon. IEEE Electr Insul Mag 2012;28(5):14–23. https://doi.org/10.1109/MEI.2012.6268438.
[6] Davalos RV, Miklavcic D. Electrochemotherapy (ect) and irreversible electroporation (ire)-advanced techniques for treating deep-seated tumors based on electroporation. Biomed Eng Online 2015;14(3):1–7. https://doi.org/10.1155/2019/2784516.
[7] Golberg A, Bruinsma BG, Uygun BE, Yarmush ML. Tissue heterogeneity in structure and conductivity contribute to cell survival during irreversible electroporation ablation by "electric field sinks". Sci Rep 2015;5(1):1–7. https://doi.org/10.1038/srep08485.
[8] Sersa G, Cemazar M, Rudolf Z. Electrochemotherapy: advantages and drawbacks in treatment of cancer patients. Cancer Ther 2003;1(133):142.
[9] Yarmush ML, Golberg A, Serša G, Kotnik T, Miklavčič D. Electroporation-based technologies for medicine: principles, applications, and challenges. Annu Rev Biomed Eng 2014;16:295–320. https://doi.org/10.1146/annurev-bioeng-071813-104622.
[10] Mir LM, Gehl J, Sersa G, Collins CG, Garbay JR, Billard V, et al. Standard operating procedures of the electrochemotherapy: instructions for the use of bleomycin or cisplatin administered either systemically or locally and electric pulses delivered by the cliniporatorTM by means of invasive or non-invasive electrodes. Eur J Cancer 2006;4(11):14–25. https://doi.org/10.1016/j.ejcsup.2006.08.003.
[11] Gehl J, Sersa G, Matthiessen LW, Muir T, Soden D, Occhini A, et al. Updated standard operating procedures for electrochemotherapy of cutaneous tumours and skin metastases. Acta Oncol 2018;57(7):874–82. https://doi.org/10.1080/0284186X.2018.1454602.
[12] Kos B, Zupanic A, Kotnik T, Snoj M, Sersa G, Miklavcic D. Robustness of treatment planning for electrochemotherapy of deep-seated tumors. J Membr Biol 2010;236(1):147–53. https://doi.org/10.1007/s00232-010-9274-1.
[13] Miklavcic D, Snoj M, Zupanic A, Kos B, Cemazar M, Kropivnik M, et al. Towards treatment planning and treatment of deep-seated solid tumors by electrochemotherapy. Biomed Eng Online 2010;9(1):1–12. https://doi.org/10.1186/1475-925X-9-10.
[14] Pavliha D, Kos B, Županič A, Marčan M, Serša G, Miklavčič D. Patient-specific treatment planning of electrochemotherapy: procedure design and possible pitfalls. Bioelectrochem 2012;87:265–73. https://doi.org/10.1016/j.bioelechem.2012.01.007.
[15] Miklavčič D, Beravs K, Šemrov D, Čemažar M, Demšar F, Serša G. The importance of electric field distribution for effective in vivo electroporation of tissues. Biophys J 1998;74(5):2152–8. https://doi.org/10.1016/S0006-3495(98)77924-X.
[16] Miklavcic D, Corovic S, Pucihar G, Pavselj N. Importance of tumour coverage by sufficiently high local electric field for effective electrochemotherapy. Eur J Cancer 2006;4(11):45–51. https://doi.org/10.1016/j.ejcsup.2006.08.006.
[17] Čorović S, Al Sakere B, Haddad V, Miklavčič D, Mir LM. Importance of contact surface between electrodes and treated tissue in electrochemotherapy. Technol Cancer Res Treat 2008;7(5):393–9. https://doi.org/10.1177/153303460800700507.
[18] Suzuki DO, Berkenbrock JA, de Oliveira KD, Freytag JO, Rangel MM. Novel application for electrochemotherapy: immersion of nasal cavity in dog. Artif Organs 2017;41(8):767–73. https://doi.org/10.1111/aor.12858.

[19] Taques MM, Guedert R, Moreno K, Rangel MMM, Suzuki DOH. Adjuvant electrochemotherapy after debulking in canine bone osteosarcoma infiltration. Artif Organs 2021;45(3):309–15. https://doi.org/10.1111/aor.13820.
[20] Lopes LB, Pintarelli GB, Dos Santos CSF, Suzuki DOH. Computer optimization of conductive gels for electrochemotherapy. Med Eng Phys 2021;98:133–9. https://doi.org/10.1016/j.medengphy.2021.10.011.
[21] Miklavčič D, Serša G, Brecelj E, Gehl J, Soden D, Bianchi G, et al. Electrochemotherapy: technological advancements for efficient electroporation-based treatment of internal tumors. Med Biol Eng Comput 2012;50(12):1213–25. https://doi.org/10.1007/s11517-012-0991-8.
[22] Maglietti F, Tellado M, Olaiz N, Michinski S, Marshall G. Minimally invasive electrochemotherapy procedure for treating nasal duct tumors in dogs using a single needle electrode. Radiol Oncol 2017;51(4):422–30. https://doi.org/10.1515/raon-2017-0043.
[23] Campana LG, Dughiero F, Forzan M, Rossi CR, Sieni E. A prototype of a flexible grid electrode to treat widespread superficial tumors by means of electrochemotherapy. Radiol Oncol 2016;50(1):49–57. https://doi.org/10.1515/raon-2016-0013.
[24] Oey I, Faridnia F, Leong SY, Burritt DJ, Liu T. Determination of pulsed electric fields effects on the structure of potato tubers. In: Miklavcic D, editor. Handbook of electroporation. Cham, Switzerland: Springer International Publishing; 2016. p. 1489–507.
[25] Corovic S, Zupanic A, Miklavcic D. Numerical modeling and optimization of electric field distribution in subcutaneous tumor treated with electrochemotherapy using needle electrodes. IEEE Trans Plasma Sci 2008;36(4):1665–72. https://doi.org/10.1109/TPS.2008.2000996.
[26] Lacković I, Magjarević R, Miklavčič D. Three-dimensional finite-element analysis of Joule heating in electrochemotherapy and in vivo gene electrotransfer. IEEE Trans Dielectr Electr Insul 2009;16(5):1338–47. https://doi.org/10.1109/TDEI.2009.5293947.
[27] Neal R, Rossmeisl J, D'alfonso V, Robertson J, Garcia P, Elankumaran S, et al. In vitro and numerical support for combinatorial irreversible electroporation and electrochemotherapy glioma treatment. Ann Biomed Eng 2014;42(3):475–87. https://doi.org/10.1007/s10439-013-0923-2.
[28] Corovic S, Lackovic I, Sustaric P, Sustar T, Rodic T, Miklavcic D. Modeling of electric field distribution in tissues during electroporation. Biomed Eng Online 2013;12(1):1–27. https://doi.org/10.1186/1475-925X-12-16.
[29] Andrade DLLS, Guedert R, Pintarelli GB, Rangel MMM, Oliveira KD, Quadros PG, et al. Electrochemotherapy treatment safety under parallel needle deflection. Sci Rep 2022;12(1):2766. https://doi.org/10.1038/s41598-022-06747-x.
[30] Sel D, Cukjati D, Batiuskaite D, Slivnik T, Mir LM, Miklavcic D. Sequential finite element model of tissue electropermeabilization. IEEE Trans Biomed Eng 2005;52(5):816–27. https://doi.org/10.1109/TBME.2005.845212.
[31] Pavselj N, Bregar Z, Cukjati D, Batiuskaite D, Mir LM, Miklavcic D. The course of tissue permeabilization studied on a mathematical model of a subcutaneous tumor in small animals. IEEE Trans Biomed Eng 2005;52(8):1373–81.
[32] Suárez C, Soba A, Maglietti F, Olaiz N, Marshall G. The role of additional pulses in electropermeabilization protocols. PLoS ONE 2014;9(12):e113413.
[33] Berkenbrock JA, Brasil Pintarelli G, de Castro Antônio Júnior A, Suzuki DOH. Verification of electroporation models using the potato tuber as in vitro simulation. J Med Bioeng 2019;39(2):224–9. https://doi.org/10.1007/s40846-018-0408-8.
[34] Pintarelli G, Berkenbrock J, Rassele A, Rangel M, Suzuki D. Computer simulation of commercial conductive gels and their application to increase the safety of electrochemotherapy treatment. Med Eng Phys 2019;74:99–105. https://doi.org/10.1016/j.medengphy.2019.09.016.
[35] Bisceglia B, de Terlizzi F, Scaglione A, Tallarino NF. Electroporation of bone cancer: numerical evaluation of the electric field in treated tissues. Compel 2013. https://doi.org/10.1108/COMPEL-11-2012-0305.
[36] Tam AL, Abdelsalam ME, Gagea M, Ensor JE, Moussa M, Ahmed M, et al. Irreversible electroporation of the lumbar vertebrae in a porcine model: is there clinical-pathologic evidence of neural toxicity? Radiology 2014;272(3):709–19.
[37] Yoo TS, Ackerman MJ, Lorensen WE, Schroeder W, Chalana V, Aylward S, et al. Engineering and algorithm design for an image processing API: a technical report on ITK-the insight toolkit. Stud Health Technol Inform 2002;85:586–92. https://doi.org/10.3233/978-1-60750-929-5-586.
[38] McCormick M, Liu X, Jomier J, Marion C, Ibanez L. Itk: enabling reproducible research and open science. Front Neuroinform 2014;8:13. https://doi.org/10.3389/fninf.2014.00013.
[39] Marty M, Sersa G, Garbay JR, Gehl J, Collins CG, Snoj M, et al. Electrochemotherapy–an easy, highly effective and safe treatment of cutaneous and subcutaneous metastases: results of esope (European standard operating procedures of electrochemotherapy) study. Eur J Cancer Suppl 2006;4(11):3–13. https://doi.org/10.1016/j.ejcsup.2006.08.002.
[40] Testori A, Tosti G, Martinoli C, Spadola G, Cataldo F, Verrecchia F, et al. Electrochemotherapy for cutaneous and subcutaneous tumor lesions: a novel therapeutic approach. Dermatol Ther 2010;23(6):651–61. https://doi.org/10.1111/j.1529-8019.2010.01370.x.
[41] Maglietti F, Tellado M, Impellizeri J. Electrodes for unique anatomical access in electroporation. In: Electroporation in veterinary oncology practice: electrochemotherapy and gene electrotransfer for immunotherapy; 2021. p. 307–19.
[42] Zupanic A, Kos B, Miklavcic D. Treatment planning of electroporation-based medical interventions: electrochemotherapy, gene electrotransfer and irreversible electroporation. Phys Med Biol 2012;57(17):5425. https://doi.org/10.1088/0031-9155/57/17/5425.
[43] Vera-Tizatl AL, Vera-Tizatl CE, Vera-Hernández A, Leija-Salas L, Rodríguez S, Miklavčič D, et al. Computational feasibility analysis of electrochemotherapy with novel needle-electrode arrays for the treatment of invasive breast ductal carcinoma. Technol Cancer Res Treat 2018:17. https://doi.org/10.1177/1533033818794939.
[44] Sano MB, DeWitt MR, Teeter SD, Xing L. Optimization of a single insertion electrode array for the creation of clinically relevant ablations using high-frequency irreversible electroporation. Comput Biol Med 2018;95:107–17. https://doi.org/10.1016/j.compbiomed.2018.02.009.
[45] Zhao Y, McKillop IH, Davalos RV. Modeling of a single bipolar electrode with tines for irreversible electroporation delivery. Comput Biol Med 2022;142:104870. https://doi.org/10.1016/j.compbiomed.2021.104870.
[46] Pagano PJT, Rodrigues J, de Lourdes Luna Santana de Andrade D, Pintarelli GB, Rodrigues J, Suzuki D. Computational study of electric field treatment at bone-neighboring tumor. In: Proceedings of the 26th international congress of mechanical engineering. ABCM; 2021.
[47] Soden DM, Larkin JO, Collins CG, Tangney M, Aarons S, Piggott J, et al. Successful application of targeted electrochemotherapy using novel flexible electrodes and low dose bleomycin to solid tumours. Cancer Lett 2006;232(2):300–10. https://doi.org/10.1016/j.canlet.2005.03.057.
[48] Berkenbrock JA, Machado RG, Suzuki DOH. Electrochemotherapy effectiveness loss due to electric field indentation between needle electrodes: a numerical study. J Healthc Eng 2018:2018. https://doi.org/10.1155/2018/6024635.
[49] Staal LG, Gilbert R. Generators and applicators: equipment for electroporation. In: Kee ST, Gehl J, Lee EW, editors. Clinical aspects of electroporation. New York: Springer; 2011. p. 45–65.
[50] Rebersek M, Miklavcic D, Bertacchini C, Sack M. Cell membrane electroporation-part 3: the equipment. IEEE Electr Insul Mag 2014;30(3):8–18. https://doi.org/10.1109/MEI.2014.6804737.
[51] Ongaro A, Campana L, De Mattei M, Dughiero F, Forzan M, Pellati A, et al. Evaluation of the electroporation efficiency of a grid electrode for electrochemotherapy: from numerical model to in vitro tests. Technol Cancer Res Treat 2016;15(2):296–307. https://doi.org/10.1177/1533034615582350.
[52] Kranjc M, Bajd F, Serša I, de Boevere M, Miklavčič D. Electric field distribution in relation to cell membrane electroporation in potato tuber tissue studied by magnetic resonance techniques. Innov Food Sci Emerg Technol 2016;37:384–90.
[53] Ivorra A, Rubinsky B. In vivo electrical impedance measurements during and after electroporation of rat liver. Bioelectrochem 2007;70(2):287–95. https://doi.org/10.1016/j.bioelechem.2006.10.005.
[54] Weinert R, Pereira E, Ramos A. Inclusion of memory effects in a dynamic model of electroporation in biological tissues. Artif Organs 2019;43(7):688–93. https://doi.org/10.1111/aor.13415.
[55] Tellado MN, Maglietti FH, Michinski SD, Marshall GR, Signori E. Predictive factors of response to electrochemotherapy in canine oral malignant melanoma. bioRxiv; 2019. p. 727164.
[56] Nemec A, Milevoj N, Lampreht Tratar U, Serša G, Čemažar M, Tozon N. Electroporation-based treatments in small animal veterinary oral and maxillofacial oncology. Front Vet Sci 2020;7:575911.
[57] Panje WR, Sadeghi N. Endoscopic and electroporation therapy of paranasal sinus tumors. Am J Rhinol 2000;14(3):187–92.